Journal of Biomedical Optics

SPIEDigitalLibrary.org/jbo

Angular and spectrally resolved investigation of single particles by darkfield scattering microscopy

Thomas Rothe
Michael Schmitz
Alwin Kienle

SPIE

Angular and spectrally resolved investigation of single particles by darkfield scattering microscopy

Thomas Rothe, Michael Schmitz, and Alwin Kienle
Institut für Lasertechnologien in der Medizin und Meßtechnik, Helmholtzstr. 12, 89081 Ulm, Germany

Abstract. A darkfield scattering microscope has been constructed that enables both angular and spectrally resolved measurements of elastic scattering patterns. The comparison of the angular and spectral resolution modes is shown in detail. Angular patterns of the backscattered light by homogeneous polystyrene spheres were measured at 57 wavelengths and the diameters of the single spheres were determined by using Mie theory at each wavelength. The mean diameter values were estimated in the angular mode with a relative standard deviation of 0.25% or less. Spectral scattering patterns of the same beads were investigated and the diameters were determined and compared with the results of the angular measurements. The estimated diameter values in the angular and the spectral mode were in an excellent agreement with deviations of less than 0.20%. [DOI: 10.1117/1.JBO.17.11.117006]

Keywords: microscopy; backscattering; Mie theory; Fourier optics; angle-resolved scattering; light scattering spectroscopy.

Paper 12594 received Sep. 10, 2012; revised manuscript received Oct. 17, 2012; accepted for publication Oct. 18, 2012; published online Nov. 8, 2012.

1 Introduction

Analyzing light scattering patterns of biological samples is a field of active research with growing interest. The observation of the scattering signatures enables the characterization of structure, size, and refractive index of a sample. For the examination of single cells, a microscopic setup is crucial. Light scattering microscopy allows one to investigate particles not only spectrally resolved,[1,2] but also angular resolved.[3,4] In the literature, several other methods are shown to acquire the scattering signatures in spectral,[5] angular,[6,7] spatial,[8] or temporal resolution modes,[9] for instance. Multimodality microscopic systems combine angular and spectrally resolved measurements.[10,11] Scattering microscopy is a label-free technique which is essential for investigating biological cells.[12] The microscopy setups offer various opportunities of sample illumination. Therefore, miscellaneous setups have been reported with brightfield illumination,[10] darkfield illumination,[11] and confocal illumination.[13,14]

A novel light scattering microscopy setup with a combination of spectral and angular resolution modes is introduced in this publication. Cottrell et al.[10] and Smith and Berger[11] published similar setups. In contrast to those, the microscope shown here has several crucial advantages. The presented microscope has a unidirectional illumination, similar to angular resolved low coherence interferometry systems,[7,15] instead of a rotationally symmetric epi- or transillumination, respectively. Hence, the angular distribution of the scattered light is not integrated over the azimuthal angle and no information is lost. In addition, the orientation of the sample can be rotated with respect to the direction of illumination. These two facts are important for the characterization of nonspherical particles that scatter into a preferred direction, such as spheroidal or cylindrical samples for instance.[15,16] Furthermore, the setup shown here is a microscope with a reflected darkfield illumination, which is advantageous for the investigation of thicker samples or *in situ* measurements.[7,17] Considering Mie theory, the backward scattered light contains more information than the forward scattered light in both angular and spectral resolution mode.[18] Besides, the system presented in this contribution is based merely on elastic scattering, which is in contrast to the setup of Smith and Berger that combines Raman scattering and elastic scattering.[11]

For the understanding of the interaction of light with biological cells or tissue, the inner structures of cells can be assessed as a first approximation as spheres,[19,20] cylinders,[21] or a mixture of spheres and cylinders.[22] The scattering of light by spheres[23] and by cylinders[24] can be described analytically. Prior to investigating biological cells and tissues, the scattering microscopy setup has to be evaluated by reference samples. The scattering microscope shown here was successfully evaluated in the spectral mode by comparison with a collimated transmission setup by Schmitz et al.[25] In this contribution, the angular resolution mode is compared with the spectral resolution mode. For validation, single polystyrene beads are measured angular and spectrally resolved and the sphere diameters are determined. The conformity of angular and spectral resolution mode is verified by comparing the diameter values for each single measurement. Both methods are in a very good agreement.

2 System Design

The scattering microscopy setup is based on an inverted microscope with a reflected darkfield illumination. Thus, only light that is scattered by the sample is collected in a certain angular range that depends on the objective and the effective numerical aperture defined by the aperture stop in F' (see Fig. 1). In the following, the angles ϑ and φ are defined relative to the z-axis, which equals the optical axis of the objective.[25] The positive z-direction is the direction of the detection path. The x- and y-directions are defined by the motorized microscopy stage

Address all correspondence to: Thomas Rothe, Institut für Lasertechnologien in der Medizin und Meßtechnik, Helmholtzstr. 12, 89081 Ulm, Germany. Tel: +49 731 1429-118; E-mail: thomas.rothe@ilm.uni-ulm.de

0091-3286/2012/$25.00 © 2012 SPIE

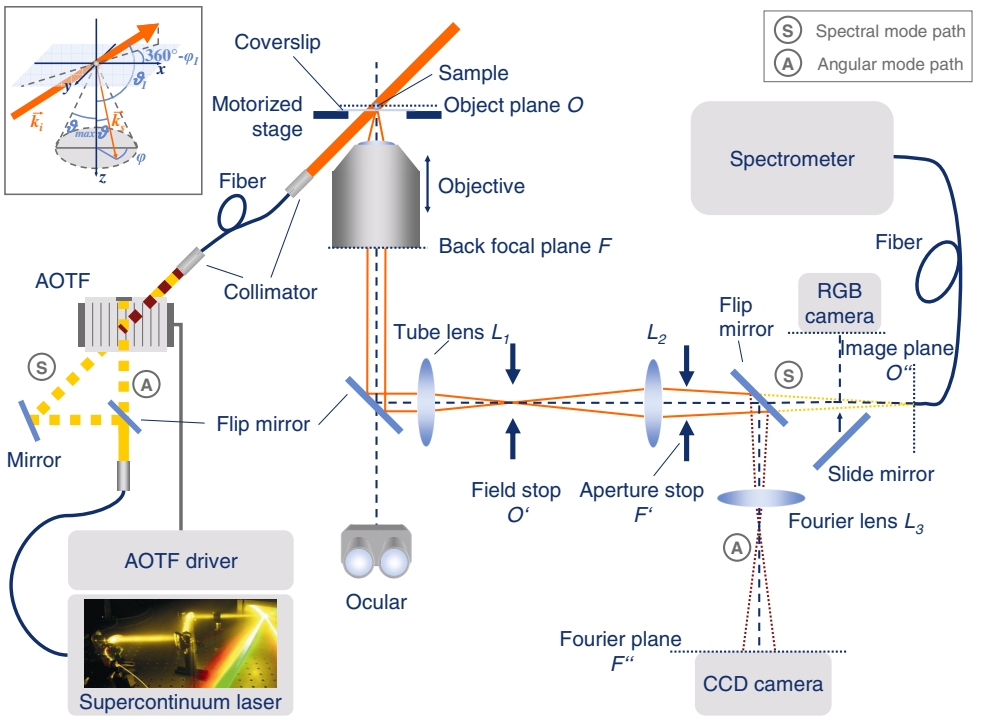

Fig. 1 Experimental setup for angular and spectrally resolved scattering microscopy. The scattered light is represented by solid orange lines. In the spectral mode path (S; dashed yellow lines), the scattered light is focused onto a fiber. In the angular mode path (A; dashed red lines), the back focal plane is focused onto a CCD camera.

(see the inset in the upper left corner in Fig. 1). So, the angle ϑ is the polar angle and φ is the azimuthal angle (in air) relative to the optical axis. As described by Schmitz et al.,[25] the unidirectional illumination is realized by a collimated beam with well-defined angles $\vartheta_I = 121$ deg and $\varphi_I = 341$ deg.

In the angular mode, a supercontinuum laser source (SuperK Blue, NKT Photonics A/S, Birkerød, Denmark) in combination with an acousto-optic tunable filter (AOTF-PCAOM Vis, Crystal Technology, LLC, Palo Alto, California) illuminates the sample placed in the object plane O quasi-monochromatically.[26] Ultrasonic waves generated by a piezoelectric transducer modulate the refractive index in the birefringent crystal of the AOTF. Hence, the incoming supercontinuum beam splits into its appropriate diffraction orders. The first diffraction order is coupled into a polarization-maintaining fiber (P1-630PM-FC-2, Thorlabs, Newton, New Jersey) and the collimated output beam of the fiber irradiates the sample. By tuning the ultrasonic frequency and power the optical wavelength can be adjusted continuously between 420 and 700 nm. In Fig. 1, the angular mode (A) is represented by dashed red lines. A part of the backscattered light by the sample is collected by the objective. In the angular mode, a long distance objective (LD EC Epiplan-Neofluar 50x/0.55 HD DIC M27 air, Carl Zeiss AG, Oberkochen, Germany) detects the scattered light in an angular range from $\Theta = 89$ deg to $\Theta = 153$ deg with an effective numerical aperture NA_{eff} of 0.53 ($\vartheta_{max} = 32$ deg). The scattering angle Θ is the angle between the incident and the scattered light. The back focal plane F of the objective represents the angular distribution of the collected scattered light. Via a lens system it is focused onto a CCD camera (SIS p1010, Theta System GmbH, Gröbenzell, Germany) placed in the Fourier plane F''. Thus, each pixel on the CCD chip indicates a certain scattering angle with a resolution of about 0.2 deg/pixel close to the optical axis. In the Fourier plane, the von Bieren condition describes the spatial frequency, i.e., the pixel position, to be proportional to $\sin(\vartheta)$,[27] where ϑ is the polar angle between the scattered light and the optical axis. The construction of the lens system is precisely described in Schmitz et al.[25] The additional Fourier lens L_3 ($f_3 = 60$ mm) is placed 100 mm behind the intermediate plane F'. The Fourier plane F'' can be found 150 mm behind L_3.

For spectrally resolved measurements, the sample is illuminated by a broadband light source provided by the supercontinuum laser. The spectral mode (S) is illustrated in Fig. 1 with dashed yellow lines. An objective with a long working distance (Epiplan 5x/0.16, Carl Zeiss AG, Oberkochen, Germany) with a numerical aperture of NA = 0.16 ($\vartheta_{max} = 9.2$ deg) detects the scattered light in an angular range from about $\Theta = 112$ deg to $\Theta = 130$ deg. One end of a fiber with a core diameter of 1000 μm is placed in the image plane O'' and connected to a CCD spectrometer (MCS-CCD-Lab, Carl Zeiss AG, Oberkochen, Germany) recording the spectrum of the detected scattered light. By sliding a mirror into the path a RGB camera (NS1300CU, NET GmbH, Finning, Germany) visualizes the object in the image plane O'', allowing the positioning of the sample with respect to the center of the fiber. With an overall magnification of 12.5× the fiber acts as a field stop with an aperture of 80 μm. A small NA is advantageous for spectrally resolved measurements since the integration over a small angular range does not average out the spectral oscillations and therefore the information content. For angular resolved measurements a high NA is favored to detect a large angular range. To alter between both, angular and spectral mode path, the AOTF is replaced and the relevant flip mirrors are toggled. Hence, without influencing the sample position, the measurement in both modes is offered smoothly.

3 Theoretical Backscattering Model Based on Mie Theory

The theoretical calculations of the angular and spectral dependencies of light scattering in this study are based on Mie theory.[24,28] It provides an exact analytical solution to Maxwell's equations describing the scattering of an electromagnetic wave by a homogeneous, spherical particle.[23] With known input parameters, Mie calculations enable the determination of the phase function $p(\Theta)$ and the scattering cross-section C_s. These input parameters are the sphere diameter D, the wavelength λ in vacuo, and the refractive indices of the scatterer n_S and of the surrounding medium n_M. The model described in Schmitz et al.[25] is valid for spectrally resolved measurements but only for air as medium surrounding the scatterer. Thus, the model was extended and generalized for calculations of light scattering by particles in an arbitrary medium with known dispersion.

The theoretical spectra and angular distributions are calculated by means of the Stokes vectors of the incident $\vec{S}_i$ and the scattered light $\vec{S}_s$, respectively. The Stokes-Mueller calculus for the scattering microscopy setup is

$$\begin{pmatrix} S_{s,0} \\ S_{s,1} \\ S_{s,2} \\ S_{s,3} \end{pmatrix} = \mathbf{T}_{\mathrm{GA}}\ \mathbf{T}_{\mathrm{MG}}\ \mathbf{M}_S\ \mathbf{R}\ \mathbf{T}_{\mathrm{GM}}\ \mathbf{T}_{\mathrm{AG}} \begin{pmatrix} S_{i,0} \\ S_{i,1} \\ S_{i,2} \\ S_{i,3} \end{pmatrix}, \tag{1}$$

where each matrix ($\mathbf{M}_S$, $\mathbf{R}$, $\mathbf{T}$) depends on the refractive indices of the scatterer and the medium. Therefore, in consideration of dispersion these Mueller matrices are dependent on the wavelength. In the following, the matrices in Eq. (1) are explained. The scattering matrix $\mathbf{M}_S$ for a single sphere is calculated by Mie theory.[25] The scattering matrix elements depend on the scattering angle Θ, the diameter of the sphere D, and the wavelength λ and are calculated as described in Bohren and Huffman.[24] All scattering angles Θ that are detectable by the presented setup can be determined from the normalized wave vectors of the incident $\vec{k}_i$ and the scattered light $\vec{k}_s$

$$\Theta = \arccos(\vec{k}_i \cdot \vec{k}_s) \tag{2}$$

with

$$\vec{k}_i = \begin{pmatrix} \sin\vartheta_i \cos\varphi_i \\ \sin\vartheta_i \sin\varphi_i \\ \cos\vartheta_i \end{pmatrix} \text{ and } \vec{k}_s = \begin{pmatrix} \sin\vartheta_s \cos\varphi_s \\ \sin\vartheta_s \sin\varphi_s \\ \cos\vartheta_s \end{pmatrix}, \tag{3}$$

where ϑ_s is the polar angle and φ_s is the azimuthal angle of the scattering direction in the medium. The incident polar angle in the medium is determined using Snell's law with $\vartheta_i = \arcsin(n_A/n_M \times \sin\vartheta_I)$, where $n_A = 1$ is the refractive index of air and n_M is the refractive index of the surrounding medium considering dispersion (refer to Sec. 4.2). The incident azimuthal angle in the medium φ_i equals the azimuthal angle in air φ_I. In the spectral mode, the value of φ_i has no influence on the spectra. Nevertheless, in the angular mode φ_i rotates the angular distribution of the scattered light and cannot be neglected. The azimuthal angle of the scattering φ_s ($\varphi_s = \varphi$) is defined in a range from 0 deg to 360 deg and is not affected by refraction. Due to the numerical aperture of the objective, the polar angle of the scattered light in the medium $\vartheta_s = \arcsin(n_A/n_M \times \sin\vartheta)$ is limited to the maximum angle of acceptance

$$\vartheta_{\max,M} = \arcsin\left(\frac{n_A}{n_M} \times \sin\vartheta_{\max}\right) \quad \text{with } \vartheta_{\max} = \arcsin(\mathrm{NA}_{\mathrm{eff}}). \tag{4}$$

These dependencies on the refractive index show the impact of dispersion on the detectable scattering angle Θ. Thus, the range of the detectable scattering angle varies with the wavelength.

The rotation matrix $\mathbf{R}$ considers the rotation of the polarization state relative to the plane of scattering spanned by the vectors $\vec{k}_i$ and $\vec{k}_s$.[24,25] The angle between the plane of scattering and the plane of incidence $\xi = \xi(\vartheta_s, \varphi_s)$ depends on the angles of the scattering direction in the medium. Hence, the rotation matrix $\mathbf{R}$ varies for each wavelength. The plane of incidence is spanned by the incident wave vector $\vec{k}_i$ and the z-axis.[25] The plane of scattering is rotated about the scattered wave vector. For $\varphi_s = \varphi_i$ and $\varphi_s = \varphi_i - 180$ deg both planes are identical.

As explained in Sec. 2, the setup is an inverted microscope with a reflected darkfield illumination where the samples are placed upon a coverslip. For that reason, the transmission through the coverslip of the illumination and the light scattered by the sample have to be considered.[25] Based on Fresnel's formulas the transmission matrices $\mathbf{T}$ have to be calculated for each interface.[29] Four matrices $\mathbf{T}$ are required, one for each interface: for the illumination the transmission matrices from air to the coverslip ($\mathbf{T}_{\mathrm{AG}}$, air to glass) and from the coverslip to the medium ($\mathbf{T}_{\mathrm{GM}}$, glass to medium) and for the light scattering the transmission back from the medium to the coverslip ($\mathbf{T}_{\mathrm{MG}}$) and from the coverslip to air ($\mathbf{T}_{\mathrm{GA}}$) have to be examined. With air as the medium surrounding the scatterer both the matrices $\mathbf{T}_{\mathrm{AG}}$ and $\mathbf{T}_{\mathrm{GM}}$ and the matrices $\mathbf{T}_{\mathrm{MG}}$ and $\mathbf{T}_{\mathrm{GA}}$ are equal. The transmission matrices are also wavelength-dependent due to dispersion. Multiple reflections between both interfaces can be neglected due to low intensity.

The detectors for both angular and spectrally resolved measurements, i.e., the CCD camera and the CCD spectrometer, are not sensitive to polarization. Thus, to determine the intensity of the scattered light, only the first Stokes parameter $S_{s,0}$ of the scattered Stokes vector $\vec{S}_s$ is of importance. The incident angles ϑ_I and φ_I are kept constant for the entire experiment. In the angular mode, the incident light is linearly polarized with $\vec{S}_i = (1 \quad -1 \quad 0 \quad 0)^{\mathrm{T}}$ since the AOTF's output is linearly polarized. The theoretical angular distribution of the scattered light is estimated for the detectable angular range by applying a single wavelength λ and the corresponding incident angles

$$I_{T,\lambda}(\vartheta, \varphi, D) = S_{s,0}(\vartheta, \varphi, \lambda, D). \tag{5}$$

The intensity $I_{T,\lambda}(u, v, D)$ for each pixel on the CCD chip with the Cartesian coordinates (u, v) is obtained via the von Bieren condition, by transforming Eq. (5) with

$$u = \sin\vartheta \cos\varphi \quad \text{and} \quad v = \sin\vartheta \sin\varphi. \tag{6}$$

The incident light for spectral measurements is unpolarized as the supercontinuum laser provides an unpolarized output. Thus, its Stokes vector is $\vec{S}_i = (1 \quad 0 \quad 0 \quad 0)^{\mathrm{T}}$. The scattered

light from all the collected angles is integrated and detected spectrally resolved. To take into account the spectral resolution of the spectrometer, the spectrum is convolved with a Gaussian function $g(\lambda)$ with a full width half maximum (FWHM) of $\Delta\lambda = 3.08$ nm, measured at the wavelength $\lambda = 632.8$ nm. By applying φ_i and ϑ_i depending on the dispersion, the theoretical scattering spectrum $I_T(\lambda, D)$ of a single sphere with diameter D measured by the scattering microscope is

$$I_T(\lambda, D) = g(\lambda) * \int_{\varphi=0}^{2\pi} \int_{\vartheta=0}^{\vartheta_{\max}} S_{s,0}(\vartheta, \varphi, \lambda, D) r^2 \sin\vartheta \mathrm{d}\vartheta \mathrm{d}\varphi, \tag{7}$$

with the distance to the detector r.

4 Materials and Methods

4.1 *Sample Preparation and Measurement*

Suspensions of polystyrene beads with a nominal Gaussian particle size distribution are investigated to measure Mie oscillations in both angular and spectral mode. Two different stock suspensions are taken as samples referred to as PS4-2 (PS/Q-F-L1086, microparticles, Berlin, Germany) and PS2-8 (PS-F-L2095, microparticles, Berlin, Germany). These suspensions have a nominal mean diameter $\nu_{\mathrm{PS4-2}} = 4.21\,\mu$m with a nominal standard deviation $\sigma_{\mathrm{PS4-2}} = 0.07\,\mu$m, and $\nu_{\mathrm{PS2-8}} = 2.82\,\mu$m with $\sigma_{\mathrm{PS2-8}} = 0.04\,\mu$m, respectively. The stock suspensions are homogenized in an ultrasonic bath for 30 min. Afterwards, the stock suspensions are diluted with distilled water to create working suspensions with a volume concentration $f_V \approx 5 \times 10^{-6}$. Thereby, it is made sure that the distances between the single particles are large enough to prevent multiple scattering. The working suspensions are given into the ultrasonic bath once more. Subsequently, a droplet of approximately 50 μl of each working suspension is placed within a sample chamber separately. The sample chamber is composed of a sandwich from a microscope slide and a coverslip. By applying adhesive tape with a thickness of about 200 μm at the boundaries, a uniform distance is provided between the microscope slide and the coverslip. Thus, reflection effects that could be detected accidentally are avoided. The sample chambers are kept with the coverslip downwards so that the polystyrene beads sink onto the coverslip.

To compare the angular resolved measurements and the spectrally resolved measurements the polystyrene beads are investigated in both modes. The sample chamber is placed onto the motorized microscope stage with the coverslip downwards. The forward scattered light by the particle could only be reflected at the upper microscope slide. However, this slide is out of focus and out of the field of view, so that these reflections are not collected by the objective. A single particle is selected manually by the operator using the motorized stage. To ensure the measurement of one single sphere the minimum distance between the investigated sphere and its nearest neighbor has to be 80 μm. This value depends on the diameter of the detection fiber and the magnification of the setup. The angular resolved measurements are performed for wavelengths between 420 and 700 nm in steps of 5 nm. First, the dark signal $I_{D,\lambda}(u, v)$ of a spot nearby the bead is measured for each wavelength to eliminate the background signal caused by the sample chamber. Then, the angular distribution of light scattered by a single particle is measured for each wavelength and for 5 positions in the field of view which is given by the field stop (see Fig. 1). For noise reduction, the measured signal of the particle $I_{P,\lambda}(u, v)$ is obtained by averaging over these 5 positions. This procedure is repeated for several particles of the working suspension. The positions of the particles are stored by the control software of the motorized stage. Therefore, the signals $I_P(\lambda)$ of exactly the same particles are measured in the spectral mode subsequently. The dark spectra $I_D(\lambda)$ of spots nearby these particles were recorded as well. For the following data analysis (Sec. 4.2) there is no necessity of measuring a reference signal, e.g., measurement of a reflectance standard, since the spectra are referenced by a polynomial fit.

4.2 *Data Analysis*

The analysis of the measured data is performed by comparison of theoretical and experimental scattering patterns. Using MATLAB (The MathWorks, Natick, Massachusetts), the theoretical patterns for the models proposed in Sec. 3 are computed. The refractive index of the polystyrene beads n_S is calculated with the dispersion formula of Tribastone and Peck.[30,31] Since water is used as the surrounding medium in the experiments, the refractive index of the medium n_M is given by a Sellmeier dispersion formula with the constants of Daimon and Masumura.[32] A set of theoretical angular patterns $I_{T,\lambda}(D, \vartheta, \varphi)$ with diameters in a range from 2 up to 5 μm with a step size of 1 nm is calculated for the aforementioned wavelengths. The experimental angular distribution is calculated by subtraction of the particles' signal $I_{P,\lambda}(u, v)$ and the dark signal $I_{D,\lambda}(u, v)$

$$I_{E,\lambda}(u, v) = I_{P,\lambda}(u, v) - I_{D,\lambda}(u, v). \tag{8}$$

In advance it was ensured that the pixel response on the incident intensity is practically identical for each pixel. Therefore, reference measurements in the angular mode are not required. To compare the theoretical and experimental angular patterns, the measured distribution depending on the pixel coordinates $I_{E,\lambda}(u, v)$ is converted to a distribution depending on the polar and azimuthal angles $I_{E,\lambda}(\vartheta, \varphi)$ utilizing Eq. (6). The correlation $C_\lambda(D)$ between theory and measurement depends on the sphere diameter and is given by

$$C_\lambda(D) = \frac{\mathrm{Cov}[I_{T,\lambda}(\vartheta, \varphi, D), I_{E,\lambda}(\vartheta, \varphi)]}{\sqrt{\mathrm{Var}[I_{T,\lambda}(\vartheta, \varphi, D)]}\sqrt{\mathrm{Var}[I_{E,\lambda}(\vartheta, \varphi)]}}, \tag{9}$$

with the covariance (Cov) and the variances (Var) of the angular distributions. The diameter termed D_λ provides the best fit of the theoretical to the experimental pattern for a certain wavelength λ and is indicated by the maximum of the correlation function $C_\lambda(D)$.

This procedure is also adopted for the spectral resolved measurements with the light-scattering microscope. A set of theoretical spectra $I_T(\lambda, D)$ is calculated for an identical range of sphere diameters and for wavelengths λ from 400 to 850 nm with a resolution of 1 nm. The dark spectrum $I_D(\lambda)$ is subtracted from the particle's spectrum $I_P(\lambda)$. Additionally, the spectrum is referenced by a tenth-order polynomial fit $I_R(\lambda)$ of the raw spectrum to account for the response of the system. This method spares the complicated measurement of a reflectance standard and is more robust. Thus, the experimental spectrum $I_E(\lambda)$ is

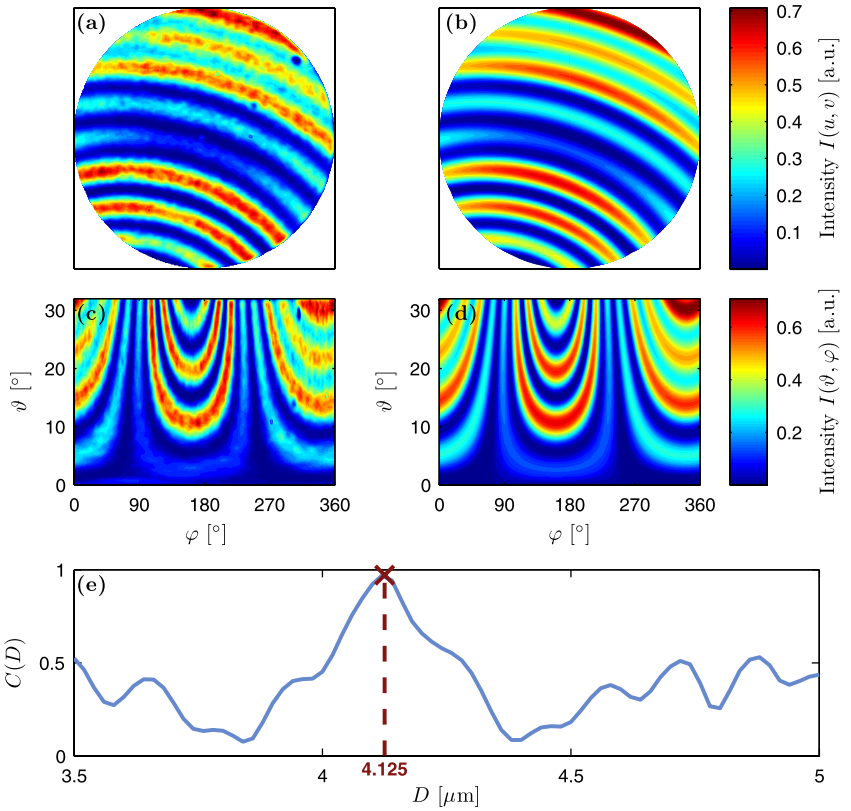

Fig. 2 Angular distribution of the scattered intensity for sample PS4-2#1 at a particular wavelength ($\lambda = 620$ nm). (a) Fourier plane measurement $I_{E,620}(u,v)$. (b) Best fit theory $I_{T,620}(u,v,D_{620})$. (c) Experimental $I_{E,620}(\vartheta,\varphi)$ and (d) theoretical $I_{T,620}(\vartheta,\varphi,D_{620})$ scattering pattern versus scattering angles. (e) Correlation function $C_{620}(D)$ with the maximum at $D_{620} = 4.125\,\mu$m.

$$I_E(\lambda) = \frac{I_P(\lambda) - I_D(\lambda)}{I_R(\lambda)} \tag{10}$$

and the correlation $C(D)$ between theoretical and experimental scattering spectrum is

$$C(D) = \frac{\mathrm{Cov}[I_T(\lambda,D), I_E(\lambda)]}{\sqrt{\mathrm{Var}[I_T(\lambda,D)]}\sqrt{\mathrm{Var}[I_E(\lambda)]}}. \tag{11}$$

The diameter of the theoretical spectrum with the maximum correlation $C(D)$ is termed D_{spec}.

5 Results and Discussion

Scattering patterns were measured on several single polystyrene beads from the working suspensions PS4-2 and PS2-8 in angular and spectrally resolved mode, respectively. In the following, the single particles are numbered and denoted with the number sign "#." The angular distribution of the scattered intensity at a particular wavelength, e.g., $\lambda = 620$ nm, for one single particle PS4-2#1 is shown in Fig. 2. In the upper left of the figure [Fig. 2(a)] the measured distribution $I_{E,620}(u,v)$ is displayed as detected with the CCD camera. Utilizing the correlation algorithm (Sec. 4.2), the sphere diameter was identified to be $D_{620} = 4.125\,\mu$m. The corresponding theoretical distribution $I_{T,620}(u,v,D_{620})$ is shown in Fig. 2(b). These two images represent the Fourier plane. In Fig. 2(c) and 2(d), the experimental pattern $I_{E,620}(\vartheta,\varphi)$ and the theoretical pattern $I_{T,620}(\vartheta,\varphi,D_{620})$ are plotted versus the angles ϑ and φ. The experimental data is normalized onto the theoretical data. Both experiment and theory are in very good agreement. The maximum of the correlation function $C_{620}(D)$ indicates the best fit, as shown in Fig. 2(e). Due to the broad peak of the correlation function, the accuracy of the diameter estimation is relatively low compared to spectrally resolved measurements. Therefore, in order to increase the accuracy, the diameter of the single particle was determined for each wavelength measured between 420 and 700 nm. The mean diameter D_{mean} is calculated by averaging these 57 estimated diameters. For PS4-2#1, the mean value is $D_{\mathrm{mean}} = 4.1200\,\mu$m and the standard deviation σ is 0.0094 μm. Consequently, by averaging the diameter values, a very high accuracy can be achieved.

To compare the two resolution modes of the scattering microscopy setup, the spectrum of the scattered light of exactly the same single particle was measured. The scatter spectrum $I_E(\lambda)$ of PS4-2#1 is represented by the light blue line in Fig. 3. Additionally, the best theoretical fit $I_E(\lambda, D_{\mathrm{spec}})$ is shown as a dark blue line. Anew, the experimental curve is normalized onto the theoretical curve. The modulation of the characteristic Mie oscillations show some dissimilarity. Nonetheless, the spectral positions of the Mie oscillations of the experimental curve coincide with the theoretical curve very well. The diameter of PS4-2#1 determined from the spectrally resolved measurement is $D_{\mathrm{spec}} = 4.128\,\mu$m. In the spectral mode, the accuracy of the diameter estimation is higher than in the angular mode. The main lobe of the correlation function in the spectral mode has a FWHM of less than 30 nm.[25] The value of D_{spec} differs slightly from the value of D_{mean}. However, the difference is less than the standard deviation σ and the diameter values show a very good agreement.

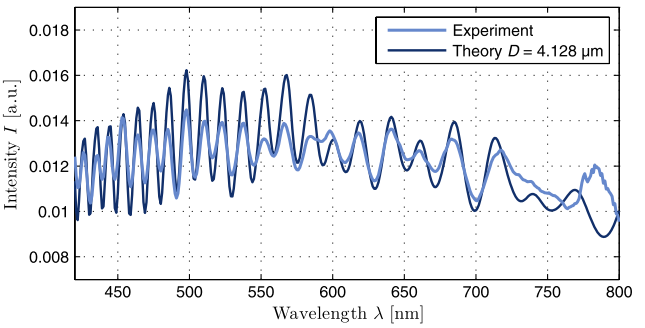

Fig. 3 Scatter spectrum $I_E(\lambda)$ of a single bead PS4-2#1 (light blue line) and theoretical spectrum $I_E(\lambda, D_{\text{spec}})$ for a sphere diameter $D_{\text{spec}} = 4.128\,\mu$m (dark blue line).

The results of the presented approach are reproducible for any single particle in the working suspension. In Fig. 4, the measured and theoretical scattering patterns for a single polystyrene bead PS2-8#5 are compared. On top of Fig. 4(a) and 4(b) the experimental $I_{E,530}(\vartheta, \varphi)$ and theoretical $I_{T,530}(\vartheta, \varphi, D_{530})$ angular distributions for the wavelength $\lambda = 530$ nm are shown with a determined sphere diameter $D_{530} = 2.742\,\mu$m. The mean diameter averaged over the wavelengths is $D_{\text{mean}} = 2.7394\,\mu$m with a standard deviation $\sigma = 0.0063\,\mu$m. In the plot below [Fig. 4(c)], the measured spectrum of PS2-8#5 is compared against the theoretical spectrum for the best fit diameter $D_{\text{spec}} = 2.739\,\mu$m. In this case, the deviation between D_{mean} and D_{spec} is merely 0.4 nm, confirming the accordance of angular and spectrally resolved measurements once more.

A statistical analysis of the results for several single particles can be performed with the help of a box plot. In the following, 5 selected single particles for each type of polystyrene beads are analyzed exemplarily. The box plots for these particles are shown in Fig. 5. They show the distribution of the estimated diameters D_λ from angular resolved measurements for each sample. The central marks in the box identify the median value of the diameters D_{median}, which is less sensitive to outliers. The median diameters D_{median} differ slightly from the mean values D_{mean}. However, Table 1 demonstrates deviations between median and mean of magnitude of 1 nm or less. The boxes themselves are limited by the lower and upper quartiles, i.e., the interquartile range characterizing the middle 50% of the diameter values. Figure 5 shows the boxes for each sample, whereas the interquartile ranges of ≈10 nm are rather small, which confirms the quality of the approach. The whiskers indicate diameter values lying outside of the interquartile range not considering outliers that are plotted individually. In addition, the diameter values D_{spec} determined from spectrally resolved measurements are marked in Fig. 5 by the asterisks. These diameters D_{spec} are located within the boxes in the most cases. A summary of the estimated sizes of the 5 exemplary particles for angular and spectral mode is given in Table 1. As previously mentioned it shows a marginal deviation of 1 nm or less between mean and median diameters. In general, for each single bead measurement the standard deviations in the angular mode are less than 10 nm, the relative standard deviations are less than 0.25%. Therefore, in the angular mode a very high accuracy in the mean diameter estimation is obtained. Furthermore the deviation between the estimated values in angular and spectral mode is less than 0.20% for PS4-2 and less than 0.13% for PS2-8, respectively. The slightly greater deviations for the samples PS4-2 may be caused by the dissimilarities between the theoretical and experimental spectra which are larger for PS4-2 than for PS2-8. The response function of the spectrometer was supposed to be a Gaussian with a FWHM of 3.08 nm for the whole spectral range, though the FWHM might depend on the wavelength, which might have a larger impact on the spectra with more

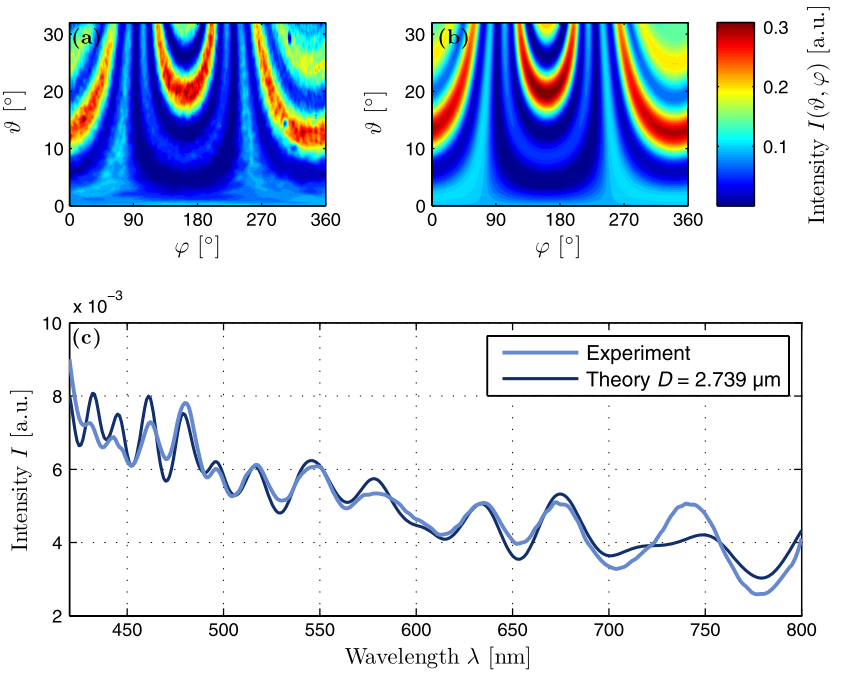

Fig. 4 Comparison of experiment and theory for sample PS2-8#5. (a) Experimental $I_{E,530}(\vartheta, \varphi)$ and (b) theoretical $I_{T,530}(\vartheta, \varphi, D_{530})$ scattering pattern versus scattering angles with $D_{530} = 2.742\,\mu$m. (c) Measured spectrum $I_E(\lambda)$ (light blue line) and theoretical spectrum $I_E(\lambda, D_{\text{spec}})$ with $D_{\text{spec}} = 2.739\,\mu$m (dark blue line).

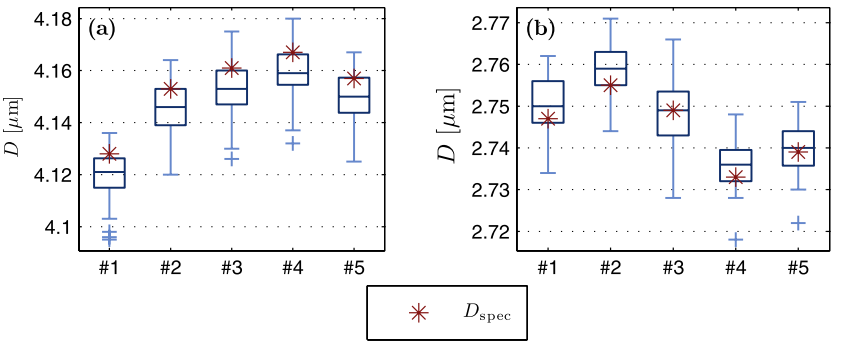

Fig. 5 (a) Statistical analysis of the estimated diameter values D_λ for 5 samples of PS4-2 and (b) 5 samples of PS2-8. Diameters determined from spectrally resolved measurements D_{spec} are plotted as red asterisks.

Table 1 Particle sizes determined in angular and spectral mode.

Sample	Sample number	Angular mode			Spectral mode
		D_{median} (μm)	D_{mean} (μm)	σ (μm)	D_{spec} (μm)
PS4-2	#1	4.121	4.1200	0.0094	4.128
	#2	4.146	4.1456	0.0096	4.153
	#3	4.153	4.1526	0.0099	4.161
	#4	4.159	4.1593	0.0096	4.167
	#5	4.150	4.1498	0.0096	4.157
PS2-8	#1	2.750	2.7506	0.0062	2.747
	#2	2.759	2.7585	0.0057	2.755
	#3	2.749	2.7487	0.0082	2.749
	#4	2.736	2.7356	0.0061	2.733
	#5	2.740	2.7394	0.0063	2.739

oscillations. However, the estimated diameter values in the angular and the spectral mode are in agreement within the measurement accuracy. In addition, the determined particle sizes are located in the range of size distributions validated with a collimated transmission setup.[25,33] The nominal values (see Sec. 4.1) given by the manufacturer appear to be overestimated.

6 Conclusion

For the evaluation of a novel scattering microscopy setup combining angular and spectral resolution mode, measurements in both modes were compared with each other. Based on elastic light scattering in the backward direction, the diameters of single polystyrene beads were distinguished. The experimental angular and spectral scattering patterns were analyzed by correlating them with the theoretical scattering patterns, which were computed by using Mie theory. In the angular mode, the diameter of a single bead was determined for multiple wavelengths and averaged subsequently. Mean diameters were calculated with a standard deviation of less than 10 nm. The relative standard deviations are 0.25% or less. By analyzing the spectrally resolved measurements, diameters of exactly the same beads were determined and compared with the diameters achieved by the angular resolved mode. The results of the investigations in angular and spectral resolution modes show an excellent agreement. The deviation between the two methods is only 0.20% or less. Thus, the combination of the angular and the spectral resolution mode results in a very high accuracy for particle characterization. In the literature other validations of angular resolved and spectroscopic scattering measurements show deviations that are 10 times larger, even though comparable suspensions were utilized.[10] The differences may originate from the differences in the setup, i.e., mode and direction of the illumination.

In this study, the investigations in the two resolution modes have figured out that changes in the particle size have stronger influence on spectral patterns than on angular patterns. These changes result in a shift or a modification of the characteristic oscillations in the scatter spectrum. The advantage of the spectral mode can be quantified with the FWHM value of the correlation functions. In contrast, the advantage of the angular resolution mode is the higher sensitivity to changes in the particle shape, structure and orientation, which will be shown in a following contribution. Preliminary experiments with cylindrical samples, e.g., fiber glass, also show a good agreement in size prediction using both methods. Therefore, the presented system with the utilization of the advantages of both angular and spectral resolution mode creates new opportunities in light scattering analysis of not only different spheres[34] but also biological samples.[11,35,36] Light scattering by cells and the contribution of the intracellular organelles could be simulated using Mie theory models with Gaussian, exponential, or log normal distributions of scatterer sizes.[37,38] These models allow the interpretation of differences in angular and spectrally resolved scattering patterns due to the internal structure of cells. Since cells or cell nuclei as well as organelles are rarely exactly spherical, analysis algorithms using Mie theory would be inappropriate. The light scattering patterns of spheroidal[15] and ellipsoidal[38] scatterers can be calculated using the T-matrix method. Scatterers of arbitrary shape could be simulated using the discrete dipole approximation.[39] The focus of future work lies on the investigations of single cells and their temporal changes, e.g., due to the induction of apoptosis in living cells.[18] Further steps are the observation of cell spheroids[40] and the comparison of these measurements with goniometric measurements.

Acknowledgments

This work is financed by the Baden-Württemberg Stiftung gGmbH and the Deutsche Forschungsgemeinschaft (DFG).

References

1. Y. Liu et al., "Elastic backscattering spectroscopic microscopy," *Opt. Lett.* **30**(18), 2445–2447 (2005).
2. A. K. Popp et al., "Microscopic origin of light scattering in tissue," *Appl. Opt.* **42**(16), 2871–2880 (2003).
3. H. Ding et al., "Fourier transform light scattering of inhomogeneous and dynamic structures," *Phys. Rev. Lett.* **101**(23), 238102 (2008).
4. H. Yu et al., "Fourier-transform light scattering of individual colloidal clusters," *Opt. Lett.* **37**(13), 2577–2579 (2012).
5. A. Amelink et al., "Single-scattering spectroscopy for the endoscopic analysis of particle size in superficial layers of turbid media," *Appl. Opt.* **42**(19), 4095–4101 (2003).
6. M. J. Berg et al., "Spatial filtering technique to image and measure two-dimensional near-forward scattering from single particles," *Opt. Express* **18**(9), 9486–9495 (2010).
7. J. W. Pyhtila et al., "Fourier-domain angle-resolved low coherence interferometry through an endoscopic fiber bundle for light-scattering spectroscopy," *Opt. Lett.* **31**(6), 772–774 (2006).
8. A. Kienle et al., "Light propagation in dry and wet softwood," *Opt. Express* **16**(13), 9895–9906 (2008).
9. T. Namita, Y. Kato, and K. Shimizu, "CT imaging of diffuse medium by time-resolved measurement of backscattered light," *Appl. Opt.* **48**(10), D208–D217 (2009).
10. W. J. Cottrell, J. D. Wilson, and T. H. Foster, "Microscope enabling multimodality imaging, angle-resolved scattering, and scattering spectroscopy," *Opt. Lett.* **32**(16), 2348–2350 (2007).
11. Z. J. Smith and A. J. Berger, "Validation of an integrated Raman- and angular-scattering microscopy system on heterogeneous bead mixtures and single human immune cells," *Appl. Opt.* **48**(10), D109–D120 (2009).
12. I. Itzkan et al., "Confocal light absorption and scattering spectroscopic microscopy monitors organelles in live cells with no exogenous labels," *Proc. Natl. Acad. Sci.* **104**(44), 17255–17260 (2007).
13. P. Huang, M. Hunter, and I. Georgakoudi, "Confocal light scattering spectroscopic imaging system for *in situ* tissue characterization," *Appl. Opt.* **48**(13), 2595–2599 (2009).
14. C. Wang et al., "Study of back-scattering microspectrum for stomach cells at single-cell scale," *J. Biomed. Opt.* **15**(4), 040505 (2010).
15. M. Giacomelli et al., "Size and shape determination of spheroidal scatterers using two-dimensional angle resolved scattering," *Opt. Express* **18**(14), 14616–14626 (2010).
16. R. Arimoto and J. Murray, "Orientation-dependent visibility of long thin objects in polarization-based microscopy," *Biophys. J.* **70**(6), 2969–2980 (1996).
17. V. Krishnaswamy et al., "Dark-field scanning *in situ* spectroscopy platform for broadband imaging of resected tissue," *Opt. Lett.* **36**(10), 1911–1913 (2011).
18. C. S. Mulvey, C. A. Sherwood, and I. J. Bigio, "Wavelength-dependent backscattering measurements for quantitative real-time monitoring of apoptosis in living cells," *J. Biomed. Opt.* **14**(6), 064013 (2009).
19. R. Drezek, A. Dunn, and R. Richards-Kortum, "Light scattering from cells: finite-difference time-domain simulations and goniometric measurements," *Appl. Opt.* **38**(16), 3651–3661 (1999).
20. H. Fang et al., "Noninvasive sizing of subcellular organelles with light scattering spectroscopy," *IEEE J. Sel. Top. Quant.* **9**(2), 267–276 (2003).
21. A. Kienle and R. Hibst, "Light guiding in biological tissue due to scattering," *Phys. Rev. Lett.* **97**(1), 018104 (2006).
22. A. Kienle et al., "Determination of the optical properties of anisotropic biological media using an isotropic diffusion model," *J. Biomed. Opt.* **12**(1), 014026 (2007).
23. G. Mie, "Beiträge zur Optik trüber Medien, speziell kolloidaler Metallösungen," *Ann. Phys.* **330**(3), 377–445 (1908).
24. C. F. Bohren and D. R. Huffman, *Absorption and Scattering of Light by Small Particles*, Wiley, New York (1983).
25. M. Schmitz, T. Rothe, and A. Kienle, "Evaluation of a spectrally resolved scattering microscope," *Biomed. Opt. Express* **2**(9), 2665–2678 (2011).
26. T. Rothe, M. Schmitz, and A. Kienle, "Angular resolved scattering microscopy," in *Advanced Microscopy Techniques II*, P. So and E. Beaurepaire, Eds., *Proc. SPIE* **8086**, 808613 (2011).
27. W. Stößel, *Fourieroptik: Eine Einführung*, Springer, Berlin (1993).
28. P. W. Barber and S. C. Hill, *Light Scattering by Particles: Computational Methods*, World Scientific, Singapore (1998).
29. E. Collett, "Mueller-stokes matrix formulation of fresnel's equations," *Am. J. Phys.* **39**(5), 517–528 (1971).
30. C. Tribastone and W. Peck, "Designing plastic optics: new applications emerging for optical glass substitutes," in *The Photonics Design and Applications Handbook*, pp. H426–H433, Laurin Publishing, Pittsfield (1998).
31. M. Schmitz, T. Rothe, and A. Kienle, "Comparison between spectral resolved scattering microscopy and collimated transmission measurements," in *Advanced Microscopy Techniques II*, P. So and E. Beaurepaire, Eds., *Proc. SPIE* **8086**, 808614 (2011).
32. M. Daimon and A. Masumura, "Measurement of the refractive index of distilled water from the near-infrared region to the ultraviolet region," *Appl. Opt.* **46**(18), 3811–3820 (2007).
33. K. Rebner et al., "Dark-field scattering microscopy for spectral characterization of polystyrene aggregates," *Opt. Express* **18**(3), 3116–3127 (2010).
34. C. Godefroy and M. Adjouadi, "Particle sizing in a flow environment using light scattering patterns," *Part. Part. Syst. Charact.* **17**(2), 47–55 (2000).
35. D. K. Kasaragod, Z. Lu, and S. J. Matcher, "Comparative study of the angle-resolved backscattering properties of collagen fibers in bovine tendon and cartilage," *J. Biomed. Opt.* **16**(8), 080501 (2011).
36. Y. Kim et al., "Anisotropic light scattering of individual sickle red blood cells," *J. Biomed. Opt.* **17**(4), 040501 (2012).
37. J. D. Wilson and T. H. Foster, "Mie theory interpretations of light scattering from intact cells," *Opt. Lett.* **30**(18), 2442–2444 (2005).
38. J. R. Mourant et al., "Polarized angular dependent spectroscopy of epithelial cells and epithelial cell nuclei to determine the size scale of scattering structures," *J. Biomed. Opt.* **7**(3), 378–387 (2002).
39. F. Voit, J. Schäfer, and A. Kienle, "Spectral simulation approach of light scattering by biological microstructures," *AAPP | Physical, Mathematical, and Natural Sciences*, **89**, C1V89S1P092 (2011).
40. J. R. Mourant et al., "Angular dependent light scattering from multicellular spheroids," *J. Biomed. Opt.* **7**(1), 93–99 (2002).